On the Effect of Birefringence on Light Transmission in Polycrystalline Magnesium Fluoride

Tzu-Chien Wen and Dinesh K. Shetty

Materials Science and Engineering

University of Utah

Salt Lake City, Utah 84112

Abstract

Light transmission in polycrystalline magnesium fluoride was studied as a function of the mean grain size at different wavelengths. The mean grain size was varied by annealing hot-pressed billets in argon atmosphere at temperatures ranging from 600 to 800°C for 1 hour. The grain-size and grain-orientation distributions were characterized by electron back scatter diffraction. The scattering coefficients were calculated from the in-line transmittance measured at various wavelengths. The scattering coefficient of polycrystalline magnesium fluoride increased linearly with the mean grain size and inversely with the square of the wavelength of light. It is shown that these trends are consistent with theoretical models based on both a limiting form of the Raleigh-Gans-Debye (RGD) theory of particle scattering and light retardation theories that take refractive-index variations along the light path. Quantitative predictions of the theories are, however, subject to uncertainly due to the restrictive assumptions made in the theories and difficulties in representing the microstructure in the theoretical models. In particular, grain-size distribution has a significant influence on the scattering coefficient calculated using particle-scattering models.

I. Introduction

Light transmission in polycrystalline ceramics is affected by several intrinsic and extrinsic factors. The intrinsic factors include atomic bonding and crystal structure, while the extrinsic factors include surface finish, void and second-phase sizes and concentrations, and grain size in birefringent polycrystalline materials. Ionic bonding, elements of low atomic weights, cubic crystal structure, optically-smooth surfaces, low concentrations and small sizes of second phases including voids, and small grain size in non-cubic crystal structures promote high transmittance in ceramics. The effects of most of the intrinsic and extrinsic factors on light transmission in ceramics are well understood and discussed in several books and articles[1-6].

Non-cubic polycrystalline ceramics are birefringent, i.e., the refractive index varies in different crystallographic directions. In birefringent polycrystalline ceramics, such as magnesium fluoride (MgF_2, tetragonal) and alumina (Al_2O_3, hexagonal close-packed), the in-line transmittance decreases with increasing grain size.[7-13] Figure 1 shows some representative data for three polycrystalline ceramics, spinel ($MgAl_2O_3$, cubic),[14] alumina,[11] and magnesium fluoride.[9] The birefringence of these ceramics, defined by $\Delta n_{max} = (n_o - n_e)$, where n_o is the refractive index in the ordinary direction and n_e is the refractive index in the extra-ordinary direction[1], are listed in Table I. It is evident from Fig. 1 that the decrease of the in-line transmittance with grain size is most pronounced for MgF_2, which has the highest birefringence ($\Delta n_{max} = 0.012$), while the transmittance of $MgAl_2O_4$ is almost independent of the grain size because it is cubic and non-birefringent ($\Delta n_{max} = 0$). Al_2O_3 exhibits intermediate behavior ($\Delta n_{max} = 0.008$). It is pointed out here that MgF_2 exhibits the highest amount of light attenuation due to birefringent grains even though it has the lowest value of the refractive index among the three

ceramics. It is generally understood that light attenuation in birefringent polycrystalline ceramics is due to variations in the refractive index along the path of light traversing arbitrarily oriented grains. However, it cannot be explained simply by geometrical optics theory considering only light reflection and refraction at grain boundaries.[11] Apetz and van Bruggen[11] have given an excellent review of these general aspects of light transmission in birefringent ceramics.

The effect of birefringence on light transmission in polycrystalline ceramics has been treated in two different ways. Apetz and van Bruggen[11] treated a birefringent polycrystalline ceramic as a two-phase composite of isotropic spherical particles with a refractive index, n_p, dispersed in an isotropic matrix of refractive index, n_m. They assumed that the difference in the refractive indices, $\Delta n = (n_p - n_m)$, was related to the intrinsic birefringence, Δn_{max}, of the crystal, and the particle diameter, d_p, was the average grain size. Since the relative refractive index, $m = n_p/n_m$ is nearly 1 for polycrystalline alumina, they used the large particle size limiting form of the Raleigh-Gans-Debye (RGD) theory of light scattering by spherical particles. The decrease of the transmittance of polycrystalline alumina with average grain size was in good agreement with the RGD theory for the assumed material parameters, volume fraction of grains, $\phi = 0.5$, and $\Delta n = 2\Delta n_{max}/3$.

Raman and Viswanathan[15], on the other hand, treated light transmission in polycrystalline ceramics as a light retardation problem. As a light ray passes through grains of different orientations in a polycrystalline ceramic, its velocity varies in each grain and the cumulative effect of all the grains in the light path is accounted for by taking into account both the path length in each grain and the grain orientation distribution. Ranganath and Ramaseshan[16] extended the theory by including the effect of change in polarization of the light during its

passage through the polycrystalline material. There has been no attempt to date to quantitatively compare this theory with transmission measurements in polycrystalline ceramics.

Kahan et al.[17] treated wave propagation in polycrystalline ceramics using a scalar Helmholtz equation for an appropriate scalar amplitude function. They derived equations for the scattering coefficient and the Rayleigh ratioin terms of a two-point correlation function with two terms, one corresponding to pore scattering and the other for grain-boundary scattering. The variation of the measured scattering coefficient with porosity in high-density alumina (LUCALOX®) was consistent with their theory. Schroeder and Rosolowski[3] used this theory to rationalize the variations of the width of the scattering profiles with specimen thickness and grain size of high-density alumina (LUCALOX®). It is shown in this paper that the theoretical approach of Kahan et al.[17] is similar to that of Raman and Viswanathan[15] and results in similar equation for the scattering coefficient under the conditions of the experiments in this study.

The purpose of this paper is to critically examine the applicability of the particle scattering model of Apetz and van Bruggen[11] and the light retardation theory of Raman and Viswanathan[15] to light transmission in polycrystalline MgF_2. Although the effect of grain size on light transmission in polycrystalline MgF_2 has been reported in prior studies,[8,9] the data were not critically examined and compared with the theories. In this study, the in-line transmission measurements were used to assess the two theoretical approaches. It is shown that the measured variations of the scattering coefficient of MgF_2 with grain size and wavelength of light are qualitatively consistent with both the theories. Quantitative predictions of the theories, however, can vary significantly due to the uncertain values of the material parameters that appear in each model: particle (or grain) volume fraction, ϕ, and the average refractive index mismatch, Δn, in the particle light scattering model; and the grain orientation distribution and the average

refractive index variation along the light path in the light retardation theory. The paper also shows that transmittance predicted by particle-scattering models are particularly sensitive to grain-size distribution in addition to the effect of average grain size..

II. Theoretical Background

The intensity of light transmitted through a window of thickness, *t*, that partially scatters light in the bulk and reflects at the two surfaces is given by the following equation:[1]

$$I(t) = I_0\left[\frac{(1-R)^2 e^{-\gamma t}}{1-R^2 e^{-2\gamma t}}\right] \quad (1)$$

In Eq. (1), I_0 is the intensity of the incident light, R is the single-surface reflectance, and γ is the scattering coefficient that accounts for the light scattered and/or absorbed in the material. For a window with optically smooth surfaces and negligible absorption, the single-surface reflectance is given by the following equation:[1]

$$R = \left(\frac{1-n}{1+n}\right)^2 \quad (2)$$

In Eq. (2), n is the average refractive index of the window. The formulation of the scattering coefficient, γ, for grain-boundary attenuation depends on the theoretical approach used. In the following, we briefly summarize the formulations of γ for light attenuation in a birefringent polycrystalline ceramic treated as particle light scattering and wave retardation, respectively.

(1) Grain-Boundary Attenuation as Particle Light Scattering

In this approach, suggested by Apetz and van Bruggen[11], a polycrystalline ceramic consisting of birefringent crystals is treated as a two-phase composite of isotropic spherical particles (diameter, d_p, and refractive index, n_p) dispersed in a homogeneous, isotropic matrix (refractive index, n_m). Grain-boundary attenuation is treated as scattering of light by the spherical particles. In 1908, Mie[18] solved Maxwell's equation for the diffraction of a plane monochromatic wave by a homogeneous sphere surrounded by a medium of different refractive index. His solution is of the form:

$$K = K(m, x) \tag{3}$$

In Eq. (3), K is the scattering efficiency of the particle, m is the relative refractive index defined earlier, and x is the normalized particle size defined as:

$$x = \frac{\pi d_p n_m}{\lambda_0} \tag{4}$$

In Eq. (4), λ_0 is the wavelength of light in vacuum. Mie's solution for K as a function of the two fundamental parameters, m and x, consists of an infinite sum of terms involving spherical Bessel functions and associated Legendre polynomials, and can only be assessed using a software. Figure 2 shows an example of the Mie solution in the form of a plot of the scattering efficiency, K, as a function of x for a fixed value of m = 1.01 calculated using MieCalc®.[19] A value of $m \sim 1$ was used here because birefringence in polycrystalline ceramics of interest in optical applications, such as magnesium fluoride and alumina, is typically small. The scattering efficiency increases monotonically with increasing x in the range, x = 0 to 100. Above this range, it reaches a peak and oscillates around an average value of ~2.

Mie's solution is rigorous and applicable for a spherical particle of arbitrary size and refractive index relative to the medium. RGD theory is a special case of Mie theory applicable under the following conditions:[20] (1) The refractive index of the particle is close to that of the medium, i.e., $|m - 1| << 1$. (2) The 'phase shift' is small, i.e., $2x|m - 1| << 1$. And as a consequence of the above conditions, (3) the scattering efficiency is small, i.e., $K << 1$. In the regime defined by these conditions, a large particle size approximation of the RGD theory is given by the following equation:[20]

$$K = 2(m-1)^2 x^2 \tag{5}$$

The dashed line in Fig. 2 is a plot of Eq. (5). It is noted that Eq. (5) is close to the Mie solution for values of x less than about 50. Apetz and van Bruggen[11] used Eq. (5) to model the effect of birefringence on light transmission in polycrystalline alumina.

The scattering coefficient of a two-phase system consisting of monodisperse spherical particles in a homogeneous medium is obtained from the single-particle scattering efficiency using the following equation:[20]

$$\gamma = \frac{N\pi d_p^2 K}{4} \tag{6}$$

In Eq. (6), N is the number of particles per unit volume. It is emphasized here that K is the scattering efficiency for single scattering by an isolated spherical particle. Therefore, Eq. (6) is applicable to multi-particle systems only when there is no multiple scattering, i.e., for low concentrations of particles[20]. It is useful to express the scattering coefficient in terms of the volume fraction of the spherical particles, ϕ:

$$\gamma = \frac{3K\phi}{2d_p} \tag{7}$$

If we employ the analytical approximation of Eq. (5) for K and substitute for m and x, Eq. (7) for the scattering coefficient takes the following form:

$$\gamma = \frac{3\pi^2 \phi d_p \Delta n^2}{\lambda_0^2} \tag{8}$$

Equation (8) is the same as the one derived by Apetz and van Bruggen[11] where they assumed ϕ = 0.5 and $\Delta n = 2\Delta n_{max}/3$. We note here that there is uncertainly in establishing values of the two parameters, Δn and ϕ, for polycrystalline ceramics and this affects the predicted values of the scattering coefficient and light transmittance significantly.

(2) Wave Retardation Theories

Raman and Viswanathan[15] assumed a polycrystalline material to be made of uniform, cube-shaped grains with edges of length, Δ, aligned along three optical axes with refractive indices, n_1, n_2 and n_3. An incident light ray traverses the polycrystalline material in a direction parallel to one set of edges covering a total number, N, grains made up of k_1 grains of refractive index, n_1, k_2 grains of refractive index, n_2 and k_3 grains of refractive index, n_3, through a window of thickness, t. The emergent wave-train was obtained by summing waves with appropriate amplitudes and phases for all possible integral values of k_1, k_2 and k_3 subject to the relation, $k_1+k_2+k_3 = N$:

$$y = P \sum_{k_1+k_2+k_3=N} \left(\frac{N!}{k_1!\,k_2!\,k_3!} \right) \left(p_1^{k_1} p_2^{k_2} p_3^{k_3} \right) e^{\frac{2\pi i}{\lambda}[c\tau - Z - (k_1 n_1 + k_2 n_2 + k_3 n_3)\Delta]} \tag{9}$$

In Eq. (9), y is the amplitude of the emergent wave, P is a factor that accounts for the loss in intensity of light due to reflections at the grain boundaries, and p_1, p_2 and p_3 are the fractions of grains with the three optical axes, respectively, τ is time, and Z is a reference position coordinate at $\tau = 0$. It is noted that the first two terms in parentheses in Eq. (9) represent the number of ways k_1, k_2 and k_3 grains can be arranged along the optical path and the probability of occurrence of each of the arrangements, respectively. The exponential term includes the change in amplitude and phase due to light retardation arising from the variation in refractive index along the light path. A number of mathematical manipulations of Eq. (9) lead to the following equation for the transmittance:

$$\frac{I}{I_0} = P^2 e^{-\frac{4\pi^2 \Delta \sum p_2 p_3 (n_2 - n_3)^2}{\lambda_0^2} t} \tag{10}$$

Or, the scattering coefficient due to the cumulative light retardation can be written as

$$\gamma = \frac{4\pi^2 \Delta \sum p_2 p_3 (n_2 - n_3)^2}{\lambda_0^2} \tag{11}$$

It is interesting to note that Eq. (11) is essentially similar to Eq. (8) in terms of the dependence of the scattering coefficient on the parameters, particle size, d_p (or, grain size, Δ), the mismatch in the refractive index, Δn, and the wavelength of the incident light, λ_0.

The theory of Kahan et al.[17] is conceptually similar to that of Raman and Viswanathan[15], but their mathematical approach is quite different. They solve scalar Helmholtz equation with a two-point correlation function and derive a general equation for the scattering coefficient for combined grain-boundary and pore scattering. They consider grains to be oriented only in two possible orientations corresponding to the highest and the lowest refractive index of the crystal.

If pore scattering is negligible relative to grain-boundary scattering and the normalized mean grain intercept length is large ($x >> 1$), their equation for the scattering coefficient reduces to the following form:

$$\gamma = \frac{8\pi^2 \Delta(p_1 p_2)(n_1 - n_2)^2}{\lambda_0^2} \tag{12}$$

It should be noted that Eq. (12) is similar to Eq. (11) in the dependence of γ on Δn, Δ, and λ_0. The absolute values of γ differ in the two expressions because of the different assumptions of the grain orientations in the two theories. Kahan et al.[17] assumed a more restrictive grain-orientation distribution (only two orientations), while Raman and Viswanathan[15] assumed three orientations. This study will focus mainly on comparing the measured transmittance of polycrystalline MgF_2 with the theoretical formulations of the scattering coefficient, γ, based on the RGD theory (Eq. 8) and that based on the wave retardation theory (Eq. 11).

III. Experimental Procedures

(1) Processing of Dense Polycrystalline MgF_2

Dense billets of polycrystalline MgF_2 were obtained from Chung Shan Institute of Science and Technology, Taoyuan, Republic of China. The billets were processed by hot-pressing MgF_2 powder at 580ºC and 276 MPa pressure for 30 minutes. The as-hot-pressed material had an average grain size, $\overline{G} \approx 0.33$ μm. Scanning electron microscope (SEM) examination of the polished surfaces of showed no evidence of residual porosity. In order to increase the average grain size, small sections (25 x 25 x 2 mm) of the billets were annealed at temperatures varying from 600 to 800ºC for 1 hour in argon. The specimens were ground successively on SiC papers

(grit numbers, 180, 320 and 400) and polished with diamond paste with 15, 9, 6, 3 and 1μm particles on both faces. The final thickness of the specimens was 1.0 mm and the root mean square roughness (R_q), as measured with a surface profilometer, was 10 nm.

(2) Measurements of Grain Size and Orientation by Electron Backscatter Diffraction (EBSD)

The grain sizes and grain orientations in the polycrystalline MgF_2 were characterized by EBSD. The principles and applications of this technique have been described in several review articles.[21, 22] The grain orientation is determined from the characteristic electron backscatter diffraction (Kikuchi) pattern obtained from a bulk sample in an SEM equipped with EBSD hardware and software. Grain sections are mapped from the change in grain orientation across grain boundaries. This is also referred to as orientation imaging microscopy (OIM).[21] A field emission gun SEM (Phillips XL/30 FEGSEM, Eindhoven, Netherlands) equipped with a sensitive CCD camera and EBSD software (OIM Analysis and Data Collection, Version 7, EDAX) was used in the present study. The SEM was operated at 20 kV and 3 nA beam current and EBSD patterns collected at 50 or 70 nm per step and 100 steps/s. The EBSD data collected over a mapped region were transformed to an orientation image, such as the one shown in Fig. 3 for polycrystalline MgF_2 annealed at 700°C, by assigning colors to grains of different orientations as indicated by the standard projection triangle. A spatial resolution of 15 nm and an orientation resolution of 0.5-1° are typical for the EBSD teachnique.[22]

The EBSD software calculates a mean linear grain intercept length, $\overline{L}_x$, in the x-direction using the following equation:

$$\bar{L}_x = \frac{R_x P_x \delta}{N_x} \tag{13}$$

In Eq. (13), R_x is the number of rows scanned in the x direction, P_x is the number of pixels in each row, δ is the scan step distance between pixels, and N_x is the total number of grain-boundary intersections in all the rows. A mean linear grain intercept length, $\bar{L}_y$, in the y-direction was similarly calculated. In the MgF_2 investigated in this study, the two mean linear intercept lengths were nearly identical. In other words, the grains were equiaxed. Therefore, a mean linear intercept length, $\bar{L}$, was calculated as the mean of $\bar{L}_x$ and $\bar{L}_y$. A mean grain size, $\bar{G}$, was calculated from the mean linear intercept length, $\bar{L}$, using the following equation:[23]

$$\bar{G} = 1.558\bar{L} \tag{14}$$

In Eq. (14), the constant of proportionality arises from a stereological analysis that relates the average grain size of a log-normal distribution of sizes of grains in the shape of tetrakaidecahedron.[23] In addition to the mean intercept lengths, the software also provided intercept-length distributions and grain-orientation distributions from the EBSD data of a mapped region. These results are presented in Section IV.

(3) Measurements of In-Line Transmittance

In-line transmittance of the polycrystalline specimens, I/I_0, were measured using three systems: (a) single wavelength laser and detector system on an optical bench, (b) a spectrophotometer operating in a wavelength range from 0.19 to 1.1 μm, and (c) an FTIR (Fourier Transform Infra Red) operating in a wavelength range, 1.66 to 10 μm.

Figure 4 shows a schematic of the light source, specimen and detector used in the single wavelength laser and detector system. Lasers of three different wavelengths, 0.633 μm (He-Ne laser, model 1122, JDS Uniphase, Milpitas, CA), 1.064 μm (YAG laser, model 4400, Quantronix Corp., East Setauket, NY), and 3.39 μm (He-Ne laser, model R-32172, Newport, Irvine, CA) were used in the single wavelength laser measurements. A Si detector was used to measure the incident (I_0) and the transmitted (I) intensities of the 0.633 μm and 1.064 μm lasers. A PbSe detector (model PDA20H, Thor Labs, Newton, NJ) was employed with the 3.39 μm laser. The long distance between the specimen and the detector (1 m) and the small active area of the detector ensured a small solid angle, ~0.5°, for measuring the light intensities. Because of this characteristic transmittance measurements made with the single-wavelength laser and detector system are sometimes referred to as real-in-line transmittance (RIT).[11]

In-line transmittance (IT) was also measured with two commercial instruments, a spectrophotometer (UV mini-1240, Shimadzu, Japan) and an FTIR (Excalibur 3100, Varian Inc., Palo Alto, CA). The spectrophotometer had two light sources: (1) a deuterium lamp covered the wavelength range from 0.19 to 0.34 μm, and (2) a halogen lamp covered the wavelength range from 0.34 to 1.1 μm. The transmittance spectra were measured by a silicon photodiode detector at a scanning speed of 700 nm per minute and 1 nm per step. The FTIR was equipped with a ceramic filament light source, a KBr beam splitter, and a deuterated tri-glycine sulfate (DTGS) detector. The scanning parameters of the FTIR included 5 kHz scanning speed and 4 cm^{-1} resolution. Both the spectrophotometer and the FTIR had large aperture angles (3-5°).

IV. Experimental Results

(1) Sizes and Orientations of Grains in Polycrystalline MgF_2

Figure 5 shows a representative histogram of the grain intercept length distribution for MgF_2 annealed at 700°C. The mean intercept length, $\bar{L}$, for this material was 0.554 μm. The calculation of the mean was based on measurements of intercept lengths on 4051 grain sections. The intercept length distribution was positively skewed on the linear plot, i.e., there was a long tail at long intercept lengths. The mean intercept length increased from 0.216 μm for the as hot-pressed MgF_2 to 1.376 μm for the MgF_2 annealed at 800°C (see Table II). The intercept length distributions for the hot-pressed and the annealed materials were all similar in that they were all positively skewed.

Figure 6 shows a plot of the cumulative fraction of the grains, $F(\theta)$, as a function of the grain orientation angle, θ, for MgF_2 annealed at 700°C. The grain orientation was defined by the angle between the c-axis of a grain and the normal to the grain section. Grains oriented along the c-axis ($\theta = 0$) were relatively few and are shown by the blue color in Fig. 3. The line plotted in Fig. 6 represents cumulative distribution of grains for isotropic random orientation as defined by the following equation:

$$F(\theta) = \int_0^{\theta} \frac{2\pi r \sin\theta r d\theta}{2\pi r^2} = \int_0^{\theta} \sin\theta d\theta = 1 - \cos\theta \qquad (15)$$

Equation (15) is based on the idea that for random isotropic distribution of grain orientations the cumulative fraction of grains with orientations equal to and less than θ is the ratio of the surface area of a section of the sphere at an angle θ and the surface area of a hemisphere. It is noted in

Fig. 6 that grains in MgF_2 were randomly oriented and this was true for all materials including as hot-pressed MgF_2. A mean grain orientation, $\bar{\theta}$, for the isotropic random orientation was defined by the following equation:

$$\bar{\theta} = \int_0^{\pi/2} \theta f(\theta) d\theta = \int_0^{\pi/2} \theta \sin\theta d\theta = 1 \tag{16}$$

Thus, the mean grain orientation for an isotropic random distribution is 1 radian or 57.3°. The mean grain orientations measured using the EBSD software for the different MgF_2 materials are listed in Table II. The values ranged from 52.8 to 57.7° with no discernible trend with grain size or annealing temperature. The average measured value for MgF_2 was 55.1°, close to the theoretical value. This is consistent with Fig. 6.

The EBSD results were also used to define a mean square deviation of the refractive index, $\overline{\Delta n^2}$, using the following equation:

$$\overline{\Delta n^2} = \frac{1}{N}\sum_{i=1}^{N-1}\left[n(\theta_{i+1}) - n(\theta_i)\right]^2 \tag{17}$$

In Eq. (17), $n(\theta_l)$ is the refractive index of the i^{th} grain with an orientation θ_l along the path of light and $n(\theta_{l+1})$ is the refractive index of the $(i+1)^{th}$ grain with an orientation θ_{l+1}. Because of its tetragonal crystal structure MgF_2 is a uniaxial crystal and the refractive index in a crystallographic direction θ with respect to the c-axis is defined by the following equation:[24]

$$n(\theta) = \frac{n_o n_e}{\sqrt{\left(n_e^2 \cos^2\theta + n_o^2 \sin^2\theta\right)}} \tag{18}$$

In Eq. (18), n_o is the refractive index in the ordinary direction (c-axis) and n_e is the refractive index in the extraordinary direction (normal to the c-axis). Values of n_o and n_e, measured on single-crystal MgF_2 and fitted to a three-term Sellmeier-type equation by Dodge[25], are listed in Table I and used in the calculations of $\overline{\Delta n^2}$ using Eqs. (17) and (18). Representative values for $\overline{\Delta n^2}$ at the three wavelengths corresponding to the three lasers are listed in Table II. $\overline{\Delta n^2}$ decreased from 2.66 x 10^{-5} at a wavelength of λ_0 = 0.633 μm to 2.07 x 10^{-5} at λ_0 = 3.39 μm.

(2) Effect of Grain Size on Transmittance and Scattering Coefficient

Figure 7 shows plots of the transmittance (I/I_0) versus mean grain size, $\overline{G}$, for the three wavelengths, 0.633, 1.064 and 3.39 μm. The lines through the data points are 'best fits' of the following equation:

$$\frac{I}{I_0} = \left[\frac{(1-R)^2 e^{-\alpha\overline{G}}}{1-R^2 e^{-2\alpha\overline{G}}}\right] \tag{19}$$

To fit Eq. (19) to the data, the single-surface reflectance, R, was calculated from Eq. (2) using the following average refractive index for a polycrystalline material with isotropic randomly oriented grains:

$$\overline{n} = \int_0^{\pi/2} n(\theta)\sin\theta d\theta \tag{20}$$

α, a material-characteristic parameter that is dependent on wavelength, but independent of grain size, was estimated by nonlinear regression analysis. α is related to the scattering coefficient, γ, via the following equation:

$$\alpha = \frac{\gamma t}{\overline{G}} \tag{21}$$

Equation (19) fits the variation of transmittance with grain size reasonably well for all the three wavelengths. This is equivalent to a linear variation of the scattering coefficient, γ, with the mean grain size, $\overline{G}$. To illustrate this, scattering coefficients were calculated directly from transmittance, $T = (I/I_0)$, at different grain sizes and wavelengths of light using the following equation derived from Eq. (1):

$$\gamma = \frac{1}{t} ln \left[\frac{(1-R)^2}{2T} + \sqrt{R^2 + \frac{(1-R)^4}{4T^2}} \right] \tag{22}$$

Figure 8 shows plots of γ versus $\overline{G}$ at the three wavelengths of light. The plots are linear. This confirms the self-consistency of Figures 7 and 8.

(3) Effect of Light Wavelength on Scattering Coefficient

In addition to the particle or grain-size dependence, the dependence of the scattering coefficient on the wavelength of light is a key to understanding and establishing the mechanism of scattering in birefringent polycrystalline materials. Both the RGD theory (Eq. 8) and the theory of Raman and Viswanathan (Eq. 11) predict a direct inverse square dependence of γ on λ_0 with a weak dependence of $\overline{\Delta n^2}$ on λ_0. To test this dependence, $[\alpha/(t\overline{\Delta n^2})] = [\gamma/(\overline{G}\,\overline{\Delta n^2})]$ was plotted as a function of λ_0. Figure 9 shows such a plot for polycrystalline MgF_2. The line fitted through the data points is a plot of the following equation:

$$\frac{\alpha}{t\overline{\Delta n^2}} = \frac{\gamma}{\overline{G}\,\overline{\Delta n^2}} = \frac{\Omega}{\lambda_0^2} \tag{23}$$

It is evident from Figure 9 that Eq. (23) gives good fit to the data. The measured scattering coefficient varies inversely with the square of the wavelength of light.

V. Discussion

The analyses of the experimental data reported in the previous section established that the scattering coefficient in polycrystalline MgF_2 scales linearly with the mean grain size, $\overline{G}$, and inversely with the square of the wavelength of light, λ_0. These trends are, however, consistent with both the RGD theory (Eq. 8) and the theory of Raman and Viswanathan (Eq. 11) and they do not help discriminate the two theories. Therefore, the transmittance measured for different grain sizes of MgF_2 were quantitatively compared with the theoretical predictions. Figure 10 shows this comparison at the wavelength of $\lambda_0 = 0.633$ μm. In the figure, both the experimental data and the theoretical predictions are shown in terms of the following common equation:

$$\frac{I}{I_0} = \left[\frac{0.9486 e^{-\alpha \overline{G}}}{1 - 0.0006778 e^{-2\alpha \overline{G}}} \right] \tag{24}$$

The numerical factor, 0.9486, is $(1–R)^2$, where the single-surface reflectance, R, was calculated using Eq. (2) and an average polycrystalline refractive index, $\overline{n}$ = 1.3848, for MgF_2 at λ_0 = 0.633 μm. The numerical factor, 0.0006778, is the value of R^2. A value, $\alpha = \alpha_{exp}$ = 2.38 μm^{-1}, gave the 'best fit' to the experimental data (blue line in Figure 10). For the RGD theory, $\alpha = \alpha_{RGD}$ = 1.98 μm^{-1} was calculated from Eq. (8) and Eq.(21) using ϕ = 1, $d_p = \overline{G}$, t = 1000 μm, and $\Delta n^2 = \overline{\Delta n^2} = 0.00002676$, as measured by EBSD at wavelength, λ_0 = 0.633 μm (Table II). The red solid line in Figure 10 corresponds to a plot of Eq. (24) with $\alpha = \alpha_{RGD}$ = 1.98 μm^{-1}. The RGD theory slightly underestimates the effect of grain size on transmittance in polycrystalline MgF_2.

Application of the Raman and Viswanathan theory (Eq. 11) to polycrystalline MgF_2 is more challenging because of their assumptions with respect to the grain shape and the grain orientations. They assumed a polycrystalline material to be made of uniform cube-shaped grains with the cube edges aligned along the three principal optical axes, 1, 2 and 3 with the refractive indices, n_1, n_2 and n_3. One set of grain edges are parallel to the incident light. A random orientation in this context implies that the probabilities of the three optical axes being aligned in the direction of the incident light are equal. Therefore, in Eq. (11), $p_1 = p_2 = p_3 = 1/3$, and $n_1 = n_o$, and $n_2 = n_3 = n_e$ for MgF_2, a uniaxial crystal. With these assumptions, we get $\sum p_2 p_3 (n_2 - n_3)^2 = \frac{2}{9}(n_e - n_o)^2 =$ 0.00003094. Note that this value is greater than the average value measured by EBSD and used in the RGD model. The parameter, Δ, in the theory of Raman and Viswanathan[15] is both the edge length of the cube-shaped grains as well as the path length of the light in each grain. For a polycrystalline material with grains of polyhedral shape and a distribution of grain sizes, there is some uncertainty in choosing a value for Δ. It is argued here that Δ should be the mean path length of light in a grain because it is the path length in a grain in combination with the refractive index in a particular crystal direction that determines the light retardation in Raman and Viswanathan theory. Therefore, $\Delta = \bar{L} = \frac{\bar{G}}{1.558}$. Equation (11), then, yields $\alpha_{Raman} = 1.96\ \mu m^{-1}$. This is nearly identical to the value predicted by the RGD theory. The plot corresponding to this value of α is shown by the solid black line in Figure 9. This line overlaps the line corresponding to the RGD theory ($\alpha = 1.98\ \mu m^{-1}$, red line).

The assumptions of cube-shaped grains and the grains being oriented only in the directions of the principal optical axes are too restrictive and not representative of polycrystalline MgF_2. A

modification of the Raman and Viswanathan theory[15] for truly isotropic random orientation of grains with a polyhedral shape and a distribution of grain sizes is non-trivial and beyond the scope of this study. It is reasonable to argue, however, that $\overline{\Delta n^2}$ measured by EBSD represents an average value of $\sum_{i=1}^{N} p_i p_{i+1}(n_{i+1} - n_i)^2$ for MgF_2, and this N term sum should replace the three-term sum in Eq. (11). This approach gives α_{Raman} = 1.69 μm^{-1} and the corresponding prediction (dashed black line in Figure 9) is slightly above the other theoretical predictions.

It is clear from the above discussion that it is difficult to discriminate between the RGD theory and the Raman and Viswanathan theory by comparing the measured and the theoretical predictions of the variation of transmittance with the mean grain size of a birefringent polycrystalline ceramic. The theories make assumptions that are not realistic for real polycrystalline ceramics. These assumptions with respect to the grain shape and the grain orientations in the Raman and Viswanathan theory[15] were noted above. Their theory also makes the assumption that polarization of light does not change as the light propagates from grain to grain, an assumption strictly not valid for anisotropic crystals.

There are also important assumptions made in employing the RGD theory to explain the effect of birefringence on transmittance of polycrystalline ceramics. The formulation of the scattering coefficient, γ, from the single-particle scattering efficiency, K, as represented in Eq. (6), is based on two assumptions: (1) particles in a medium scatter light independently, and (2) each particle causes only single scattering[20]. Clearly, these assumptions are valid only for two-phase systems with a low concentration of the dispersed phase. van de Hulst[20] suggests that a mutual distance of 3 times the radius is a sufficient condition for independent scattering. This interparticle spacing is equivalent to a volume fraction of 0.0335. Secondly, according to van de

Hulst[20], single scattering prevails if $\gamma t < 0.1$. For polycrystalline MgF_2, $\phi \approx 1$ and γt varied from 0.74 to 5.25 with grain size for $\lambda_0 = 0.633$ μm. Only for $\lambda_0 = 3.39$ μm and $\overline{G} \leq 0.86$ μm, γt was less than 0.1. Strictly speaking, therefore, RGD theory should not be applicable to polycrystalline MgF_2. And yet, the Apetz and van Bruggen model based on the RGD theory gives a reasonable prediction of the effects of birefringence and grain size on the light transmittance of MgF_2. To resolve this dichotomy, transmittance measurements are being made on a model two-phase system, monodispersed silica spheres in a solution of water in glycerol, where the mismatch of the refractive indices is comparable to the average birefringence in polycrystalline MgF_2. The objective of this study is to establish the range of silica volume fraction where the RGD theory is applicable. These results will be presented in a future paper.

We note here in closing that the average grain size, $\overline{G}$, defined in this study is based on an arithmetic number average intercept length, $\overline{L}$. In reality, the intercept length and the grain size are both distributed, as shown by the example of Fig. 5. What is the effect of this grain-size distribution on grain-boundary scattering? To answer this question, we note that the RGD equation for the scattering coefficient, Eq. (6), which is valid for monodisperse particles, now takes the following form for polydisperse systems:

$$\gamma = \frac{3\pi^2 \Delta n^2 \sum_{i=1}^{i=N} \phi_i d_i}{\lambda_0^2} \qquad (25)$$

In Eq. (25), ϕ_i is the volume fraction of particles in a size interval with the midpoint size, d_i, and N is the total number of grain size intervals. The summation in Eq. (25) can, in fact, be identified as a volume fraction weighted average grain size:

$$\overline{G}_V = \sum_{i=1}^{i=N} \varphi_i d_i = \frac{\sum_{i=1}^{i=N} n_i d_i^4}{\sum_{i=1}^{i=N} n_i d_i^3} \tag{26}$$

In Eq. (26), n_i is the number of grains (particles) in a size interval centered at d_i. Calculations of $\overline{G}_V$ for polycrystalline MgF_2 from EBSD data revealed that $\overline{G}_V = \beta \overline{G}$, where the factor β accounts for the effect of the grain-size distribution on grain-boundary scattering. For MgF_2 heat-treated at different temperatures, β ranged from 1.89 to 2.76 with an average value of 2.32. In other words, the scattering coefficient predicted by the RGD theory is, on an average, 2.32 times greater than the one based on the number average grain size, $\overline{G}$. The theoretical prediction based on this grain-size distribution corrected RGD scattering theory is shown by the dashed red line in Figure 10. The grain-size distribution has a significant effect on the RGD theory prediction. The predicted transmittance is significantly below the measured values. It is interesting to note here that the predictions of the light retardation models are not as sensitive to grain-size distribution because there is no explicit dependence of the scattering coefficient on volume fractions of grains or particles.

.

VI. Conclusions

1. The scattering coefficient of polycrystalline MgF_2 scales linearly with grain size and inversely with the square of the wavelength of light.

2. The observed trends of the scattering coefficient with grain size and wavelength of light are consistent with both the Apetz and van Bruggen model based on the RGD theory of particle light scattering as well as the light retardation theory of Raman and Viswanathan..
3. The theoretical predictions of the transmittance in birefringent polycrystalline ceramics are subject to considerable uncertainty due to the uncertain values of the material parameters that appear in the theoretical equations.
4. Transmittance predicted by particle-scattering models, in particular, is strongly affected by grain-size distribution in addition to the average grain-size effect.

VII. References

1. D. C. Harris, *Materials for Infrared Windows and Domes: Properties and Performance*; Ch. Chapter p. 415. Edited. SPIE Optical Engineering Press: Bellingham, WA, 1999.
2. J. G. J. Peelen and R. Metselaar, "Light Scattering by Pores in Polycrystalline Materials: Transmission Properties of Alumina," *J. Appl. Phys.*, **45** [1] 216-20 (1974).
3. J. Schroeder and J. H. Rosolowski, "Light Scattering in Polycrystalline Materials," pp. 156-68. in *Emerging Optical Materials,* Vol. 297. Edited by S. Musikant. SPIE: International Society for Optics and Photonics, 1982.
4. G. H. Beall and L. R. Pinckney, "Nanophase Glass-Ceramics," *J. Am. Ceram. Soc.*, **82** [1] 5-16 (1999).
5. H. E. Bennett and J. O. Porteus, "Relation Between Surface Roughness and Specular Reflectance at Normal Incidence," *J. Opt. Soc. Am.*, **51** [2] 123-29 (1961).

6. A. Krell, J. Klimke, and T. Hutzler, "Transparent Compact Ceramics: Inherent Physical Issues," *Optical Materials,* **31** 44-50 (2009).
7. W.-Y. Lin, M.-H. Hon, and S.-J. Yang, "Effect of Grain Growth on Hot-Pressed Optical Magnesium Fluoride Ceramics," *J. Am. Ceram. Soc.,* **71** [3] C-136 - C-37 (1988).
8. C.-S. Chang, M.-H. Hon, and S.-J. Yang, "Effect of Grain Growth of Hot-Pressed Magnesium Fluoride on Optical Transmittance," *Japanese Journal of Applied Physics,* **30** [3] 506-10 (1991).
9. T.-C. Wen and D. K. Shetty, "Birefringence and Grain-Size Effects on Optical Transmittance of Polycrystalline Magnesium Fluoride," pp. 73020Z-1 - 20Z-6. in *Window and Dome Technologies and Materials XI,* Vol. 7302. Window and Dome Technologies and Materials. Edited by R. W. Tustison. SPIE: International Society for Optics and Photonics, Orlando, FL, 2009.
10. A. Krell, P. Blank, H. Ma, T. Hutzler, M. P. B. v. Bruggen, and R. Apetz, "Transparent Sintered Corundum with High Hardness and Strength," *J. Am. Ceram. Soc.,* **86** [1] 12-18 (2003).
11. R. Apetz and M. P. B. v. Bruggen, "Transparent Alumina: A Light-Scattering Model," *J. Am. Ceram. Soc.,* **86** [3] 480-86 (2003).
12. G. Bernard-Granger and C. Guizard, "Influence of Co-Doping on the Sintering Path and on the Optical Properties of a Submicronic Alumina Material," *J. Am. Ceram. Soc.,* **91** [5] 1703-06 (2008).
13. I. Yamashita, H. Nagayama, and K. Tsukuma, "Transmission Properties of Translucent Polycrystalline Alumina," *J. Am. Ceram. Soc.,* **91** [8] 2611-16 (2008).

14. A. Krell, J. Klimke, and T. Hutzler, "Advanced Spinel and Sub-μm Al_2O_3 for Transparent Armour Applications," *Journal of the European Ceramic Society*, **29** 275-91 (2009).
15. C. V. Raman and K. S. Viswanathan, "The Theory of the Propagation of Light in Polycrystalline Media," *Proc. Indian Acad. Sci. A*, **41** 37-43 (1955).
16. G. S. Ranganath and S. Ramaseshan, "Optical transmission in polycrystals," *Optica Acta*, **19** [9] 781-90 (1972).
17. H. M. Kahan, D. P. Stubbs, and R. V. Jones, "The Potentialities of Fine Grained Ceramics for Optical and Acoustical Applications," pp. 185-203. in *Optical and Acoustical Micro-Electronics*, New York, NY, 1974.
18. G. Mie, "Contibutions on the Optics of Turbid Media - Particularly Colloidal Metal Solutions," *Annalen der Physik*, **330** [3] 377-445 (1908).
19. B. Michel, MieCalc-Freely Configurable program for Light Scattering Calculations (Mie Theory), http://www.lightscattering.de/MieCalc/eindex.html, 2013.
20. H. C. v. d. Hulst, *Light Scattering by Small Particles*; Ch. Chapter p. 446. Edited. Dover Publications, Inc.: New York, 1981.
21. B. L. Adams, S. I. Wright, and K. Kunze, "Orientation Imaging: The Emergence of a New Microscopy," *Metallurgical Transactions A*, **24A** [4] 819-31 (1993).
22. F. J. Humphreys, "Review: Grain and Subgrain Characterization by Electron Backscatter Diffraction," *Journal of Materials Science*, **36** 3833-54 (2001).
23. M. I. Mendelson, "Average Grain Size in Polycrystalline Ceramics," *Journal of the American Ceramic Society*, **52** [8] 443-46 (1969).

24.A. Yariv and P. Yeh, *Optical Waves in Crystals*; Ch. Chapter p. 589. Edited by J. W. Goodman. John Wiley and Sons: New York, 1984.

25. M. J. Dodge, "Refractive Properties of Magnesium Fluoride," *Applied Optics*, **23** [12] 1980-85 (1984).

Acknowledgments

The authors acknowledge Dr. Stuart I. Wright and Mr. Ron Witt of EDAX Inc. for their assistance in collecting the EBSD data on MgF_2 specimens and Mr. Yen-Chih Lin of the Physics Department, Cornell University, for his help in measurements of refractive index of the silica spheres by the index-matching method.

Table I. The Isotropic Refractive Index of $MgAl_2O_4$ and the Refractive Indices in the Ordinary (n_o) and the Extraordinary (n_e) Directions for Al_2O_3 and MgF_2 At Different Wavelengths (From Harris[1]).

Materials	λ_0 (μm)	n_o	n_e	$\lvert\Delta n_{max}\rvert$
$MgAl_2O_4$	0.640	1.7134	1.7134	0
Al_2O_3	0.645	1.7653	1.7573	0.008
MgF_2	0.633	1.3770	1.3888	0.0118
MgF_2	1.064	1.3732	1.3848	0.0116
MgF_2	3.39	1.3560	1.3664	0.0104

Table II. Mean Grain Intercept Lengths, Mean Orientations and Mean Square Deviations of Refractive Index for Polycrystalline MgF_2.

Processing History	$\bar{L}$ (μm)	$\bar{\theta}$ (°)	$\overline{\Delta n^2}$ (x10^{-5})		
			0.633 μm	1.064 μm	3.39 μm
As Hot-Pressed #1	0.216	54.89	2.580	2.493	2.003
As Hot-Pressed #2	0.252	53.31	2.683	2.592	2.083
Annealed at 600°C	0.290	52.81	2.977	2.877	2.312
Annealed at 650°C	0.292	55.48	2.699	2.608	2.096
Annealed at 700°C	0.554	55.80	2.682	2.592	2.083
Annealed at 750°C	0.611	55.22	2.582	2.495	2.005
Annealed at 775°C	1.143	55.36	2.665	2.575	2.069
Annealed at 800°C	1.376	57.68	2.540	2.455	1.972
Average		55.07	2.676	2.586	2.078

Figure Captions

Figure 1. Variations of the transmittance of polycrystalline $MgAl_2O_4$, Al_2O_3 and MgF_2 as functions of the grain size at the indicated wavelengths (birefringence for Al_2O_3 and MgF_2 are listed in Table I).

Figure 2. Variation of the scattering efficiency (K) as a function of the normalized particle size (x) for a spherical particle in a medium with small mismatch in refractive index according to Mie theory and an approximation of the RGD theory.

Figure 3. Microstructure of polycrystalline MgF_2 annealed at 700°C for 1 hour as revealed by EBSD. The color key for orientation is shown by the standard triangle.

Figure 4. Schematic of the optical setup used in transmittance measurements using single wavelength lasers. A: laser, B: aperture, C: filter, D: specimen, E: detector.

Figure 5. Histogram of grain intercept length for polycrystalline MgF_2 annealed at 700°C for 1 hour as measured by EBSD.

Figure 6. Cumulative distribution of grain orientations in MgF_2 annealed at 700°C for 1 hour measured by EBSD compared with isotropic random distribution.

Figure 7. Variations of transmittance of polycrystalline MgF_2 with mean grain size at three different wavelengths.

Figure 8. Variations of the scattering coefficient of polycrystalline MgF_2 with mean grain size at three different wavelengths.

Figure 9. Variation of grain size normalized scattering coefficient of polycrystalline MgF_2 with wavelength of light.

Figure 10. Transmittance of polycrystalline MgF_2 as a function of grain size compared with theoretical predictions.

UU IR Author Manuscript

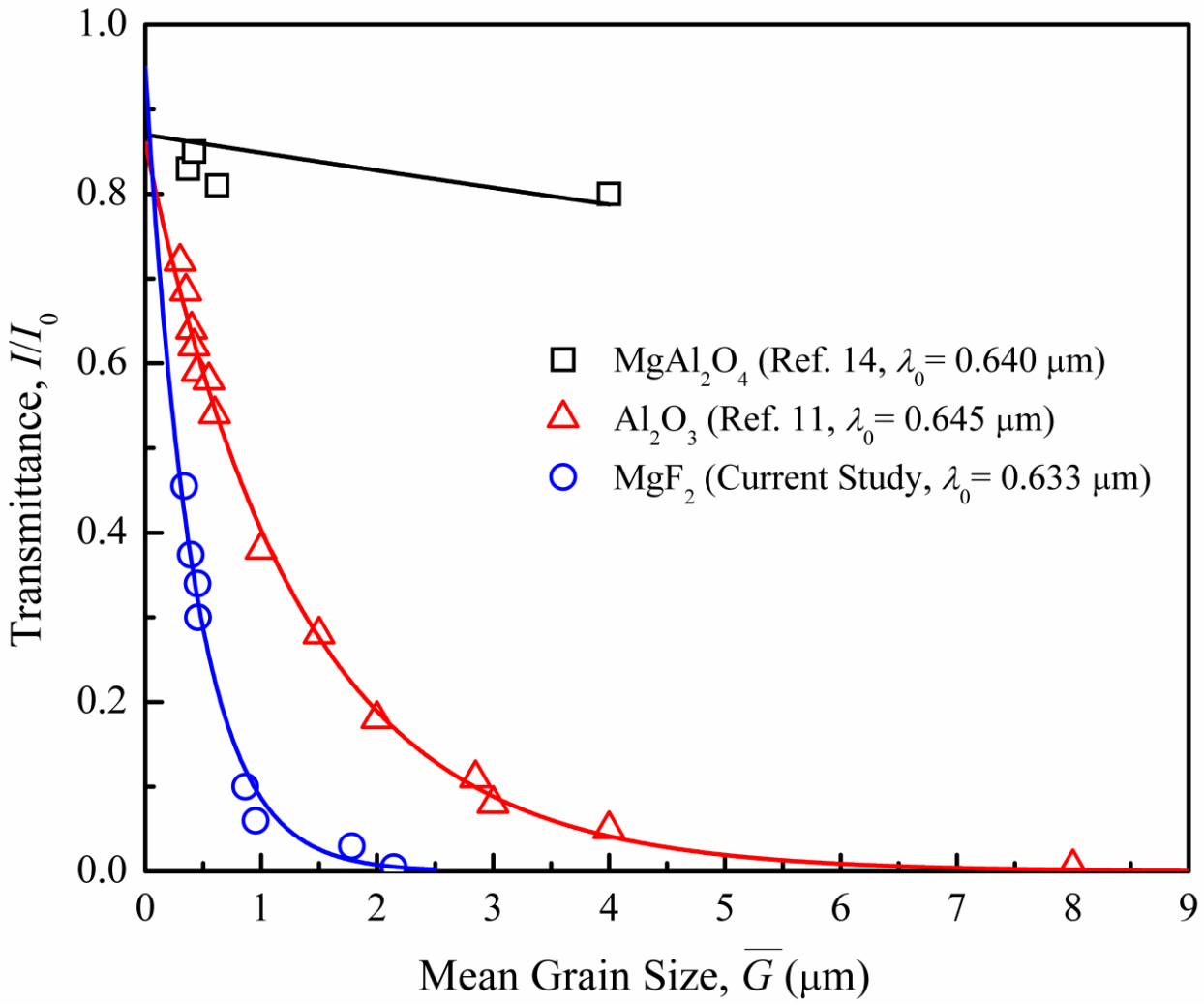

Figure 1. Variations of the transmittance of polycrystalline $MgAl_2O_4$, Al_2O_3 and MgF_2 as functions of the grain size at the indicated wavelengths (birefringence for Al_2O_3 and MgF_2 are listed in Table I).

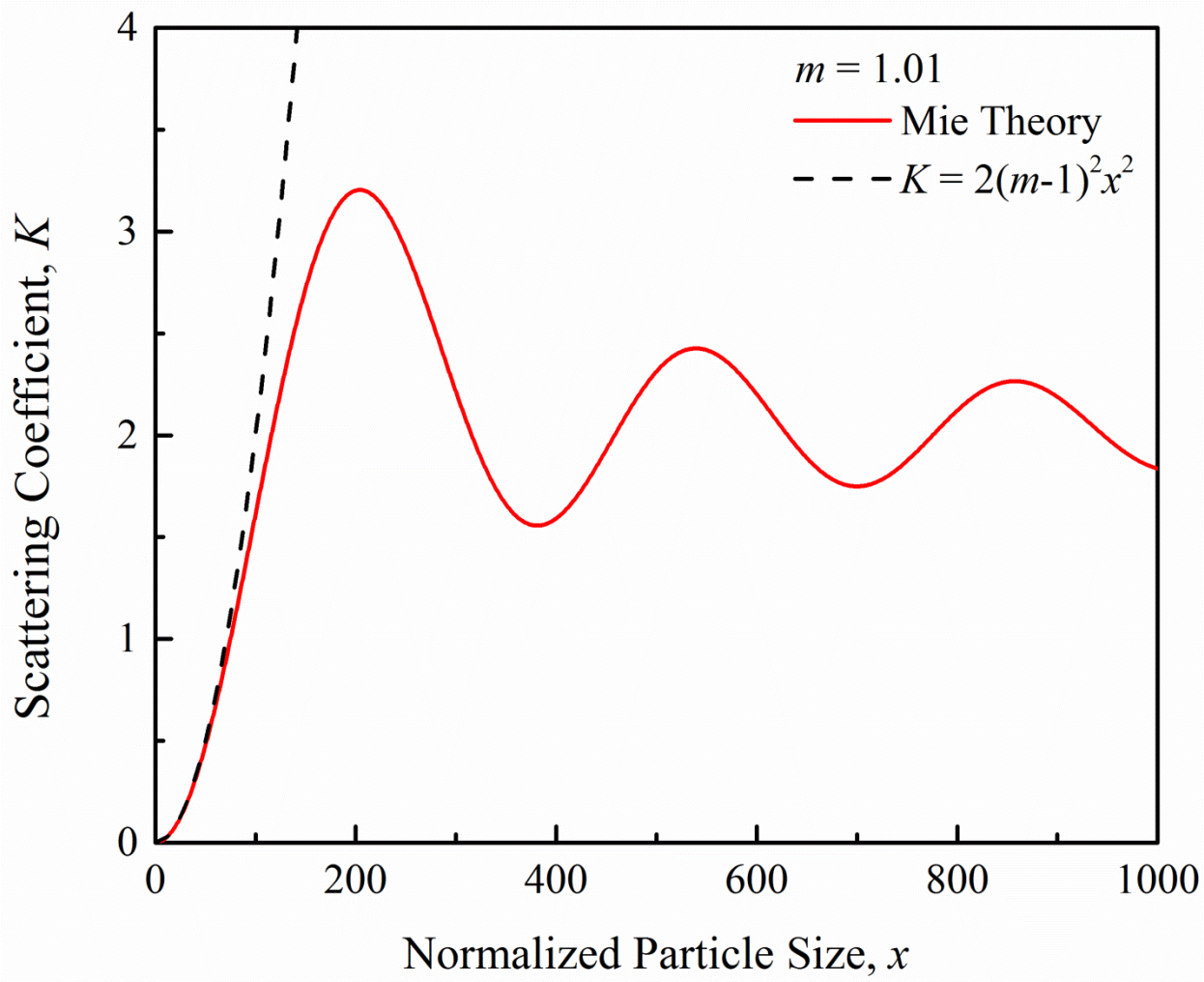

Figure 2. Variation of the scattering coefficient (K) as a function of the normalized particle size (x) for a spherical particle in a medium with small mismatch in refractive index according to Mie theory and an approximation of the RGD theory.

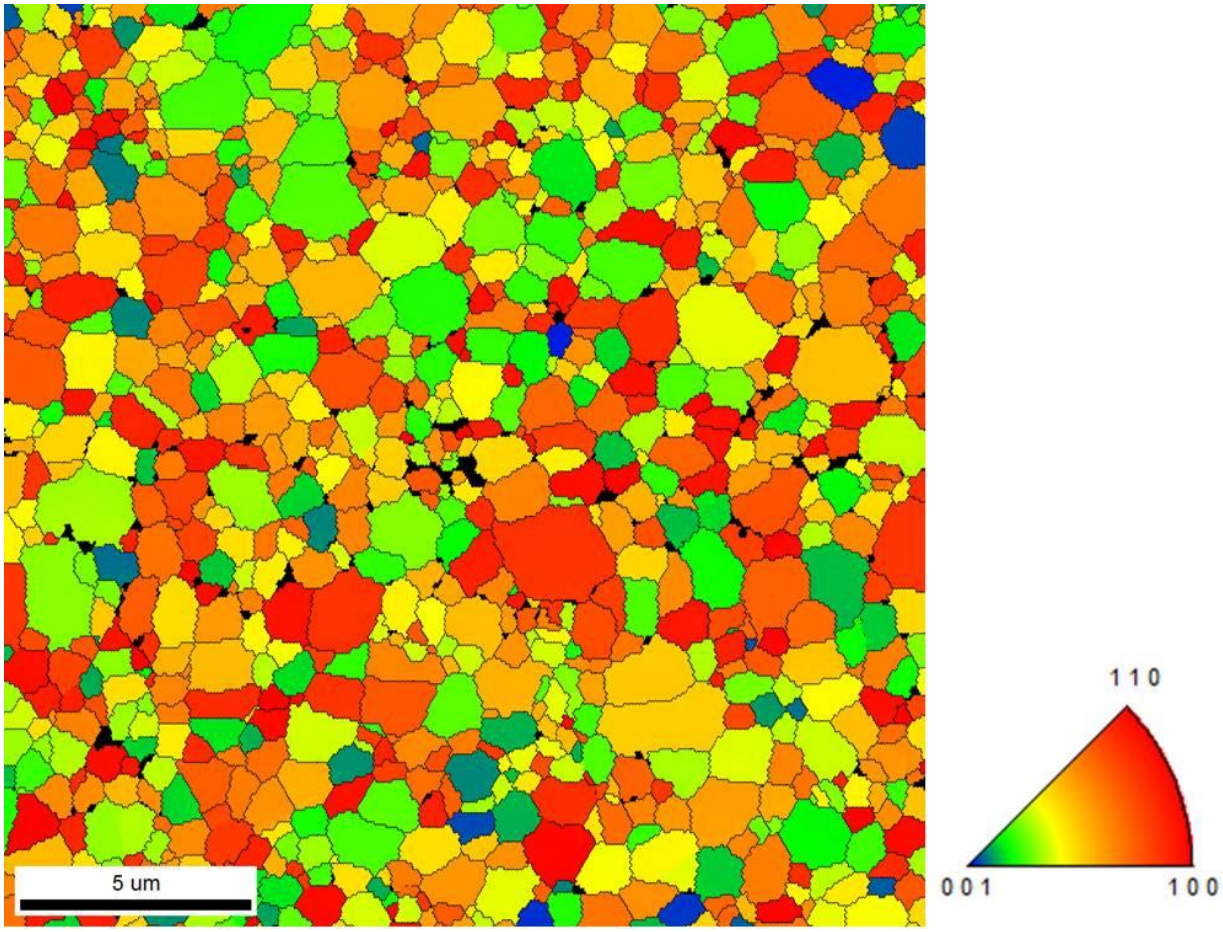

Figure 3. Microstructure of polycrystalline MgF_2 annealed at 700°C for 1 hour as revealed by EBSD. The color key for orientation is shown by the standard triangle.

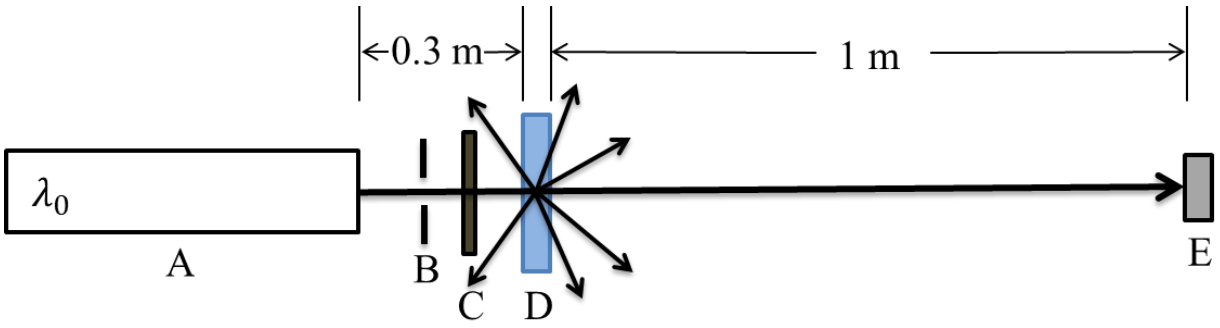

Figure 4. Schematic of the optical setup used in transmittance measurements using single wavelength lasers. A: laser, B: aperture, C: filter, D: specimen, E: detector.

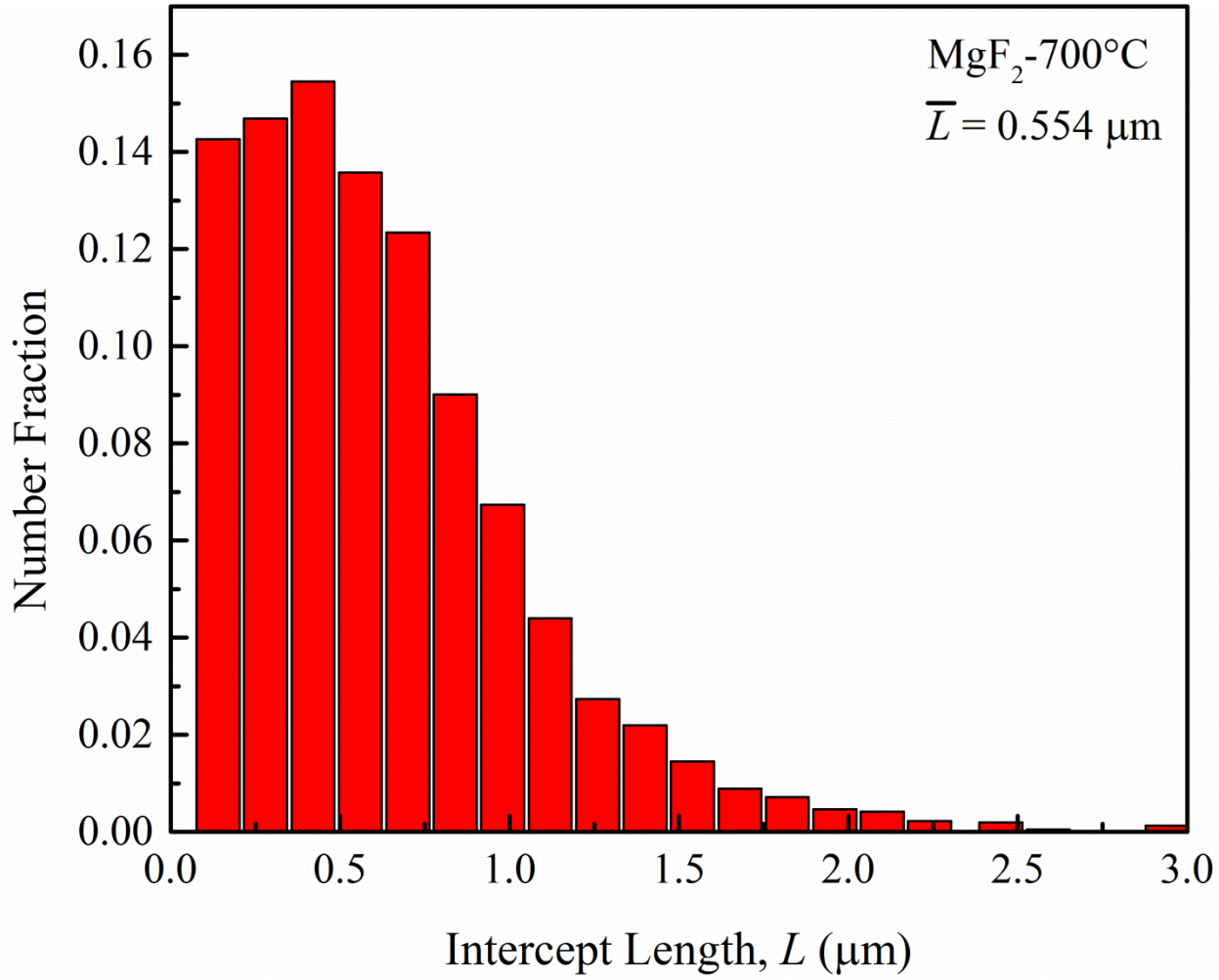

Figure 5. Histogram of grain intercept length for polycrystalline MgF_2 annealed at 700°C for 1 hour as measured by EBSD.

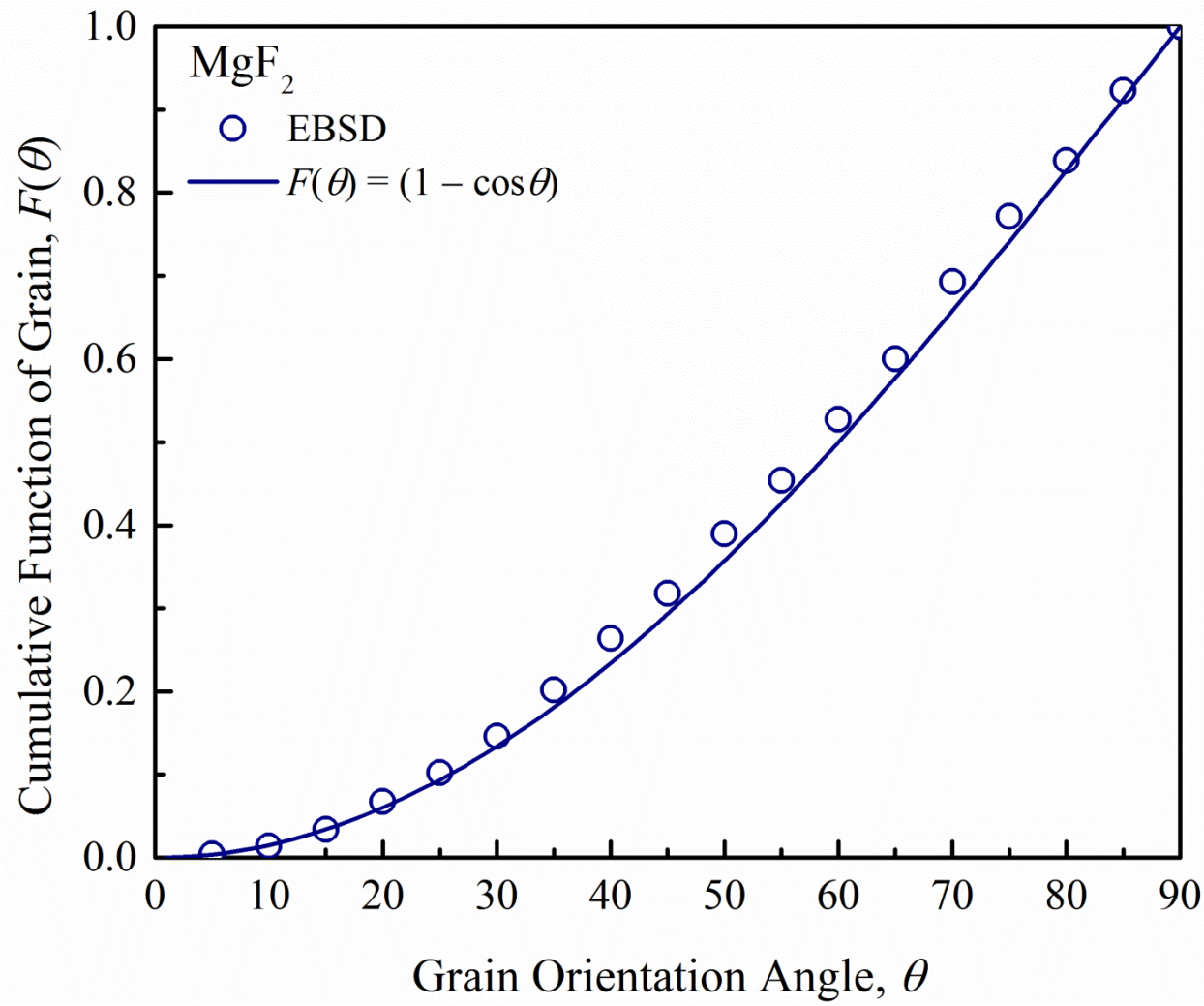

Figure 6. Cumulative distribution of grain orientations in MgF_2 annealed at 700°C for 1 hour measured by EBSD compared with isotropic random distribution.

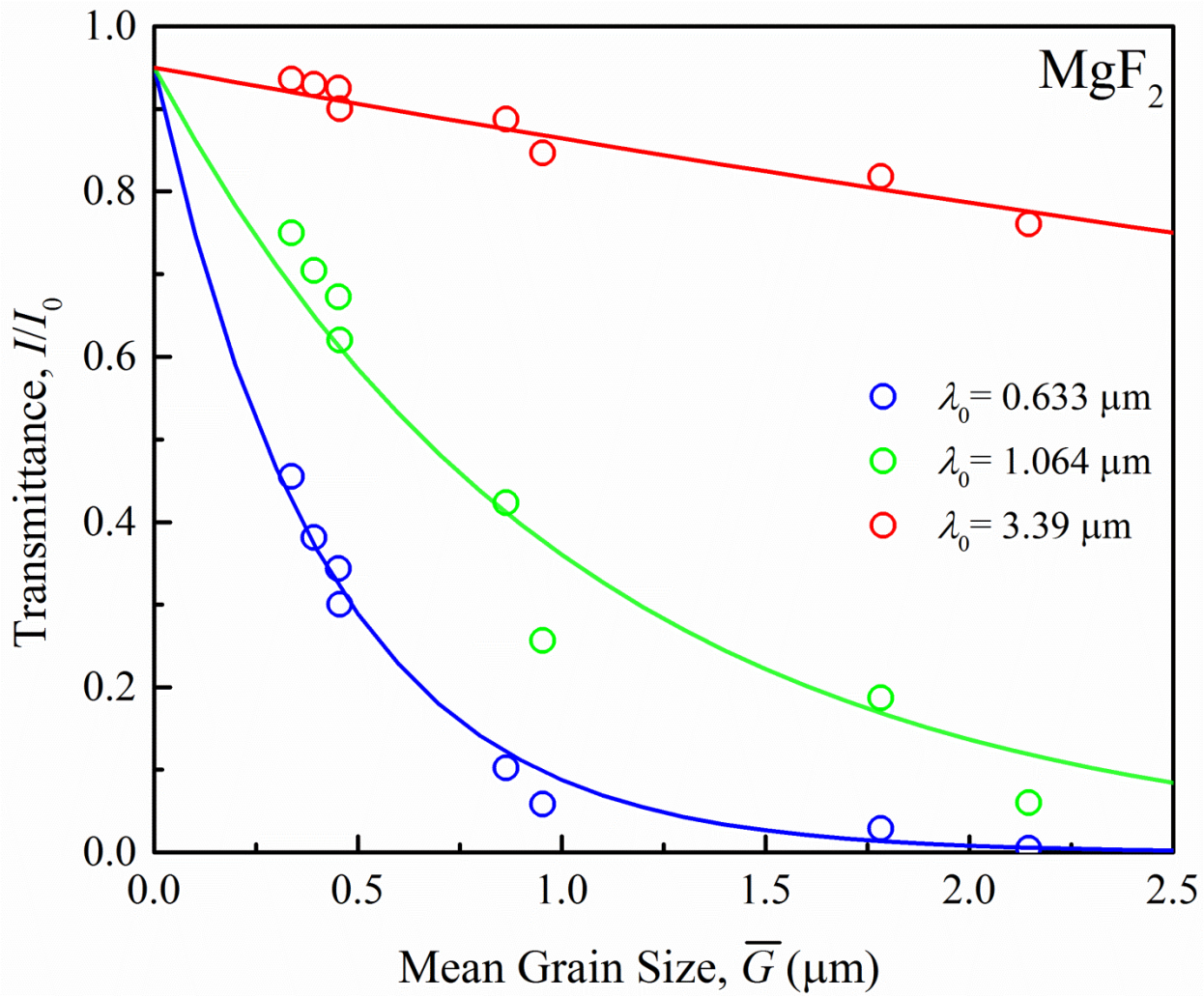

Figure 7. Variations of transmittance of polycrystalline MgF_2 with mean grain size at three different wavelengths.

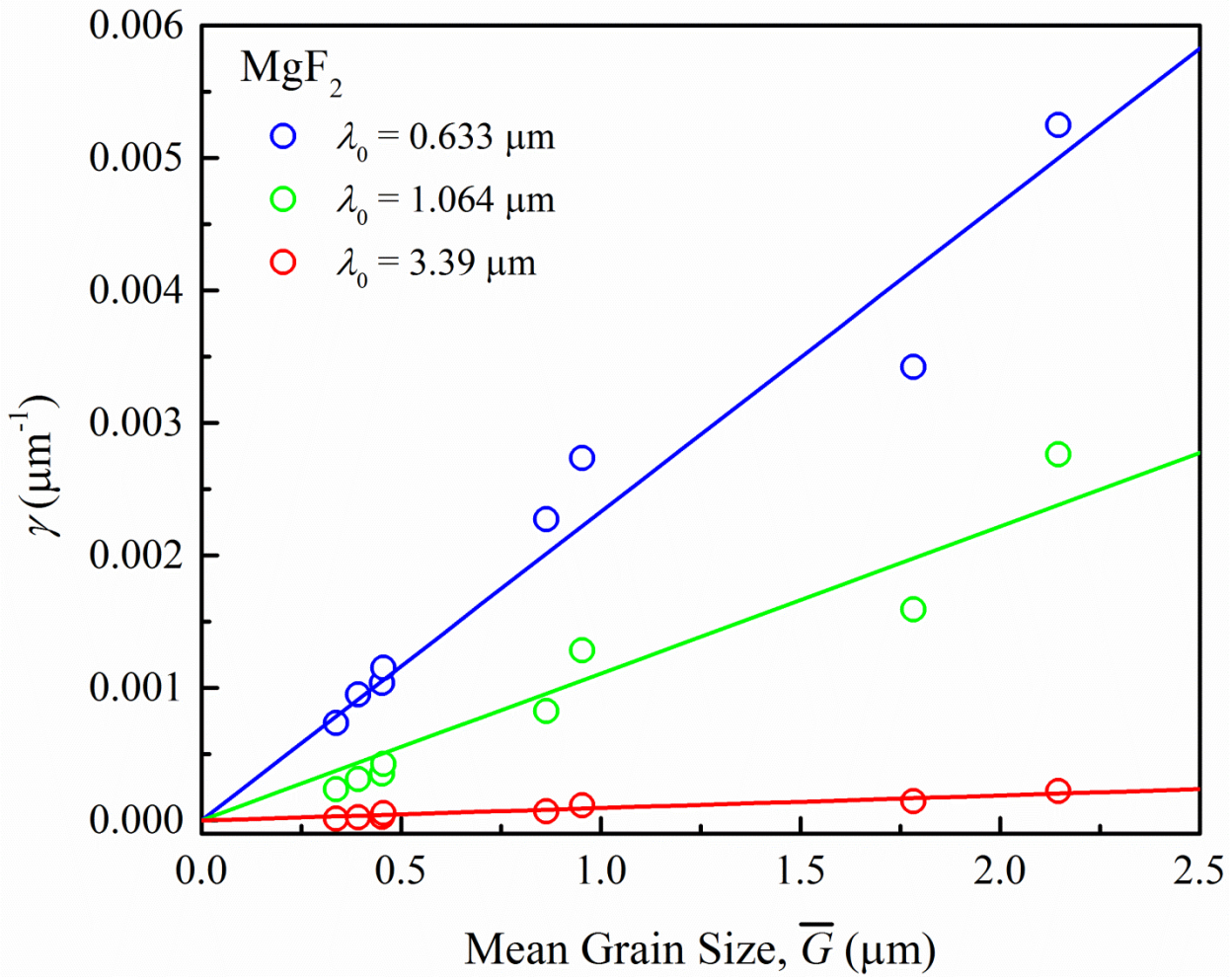

Figure 8. Variations of turbidity of polycrystalline MgF_2 with mean grain size at three different wavelengths.

UU IR Author Manuscript

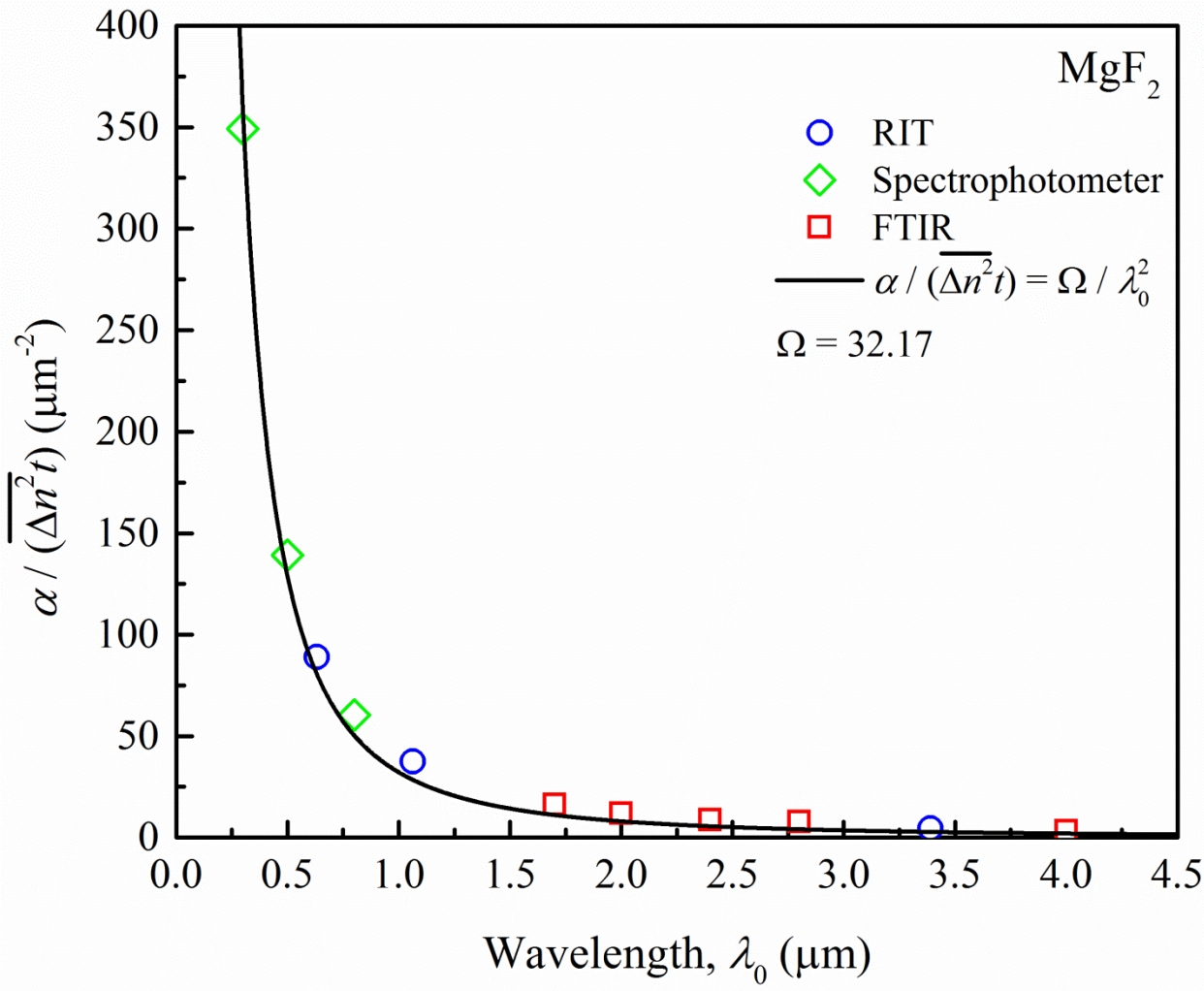

Figure 9. Variation of grain size normalized turbidity of polycrystalline MgF_2 with wavelength of light.

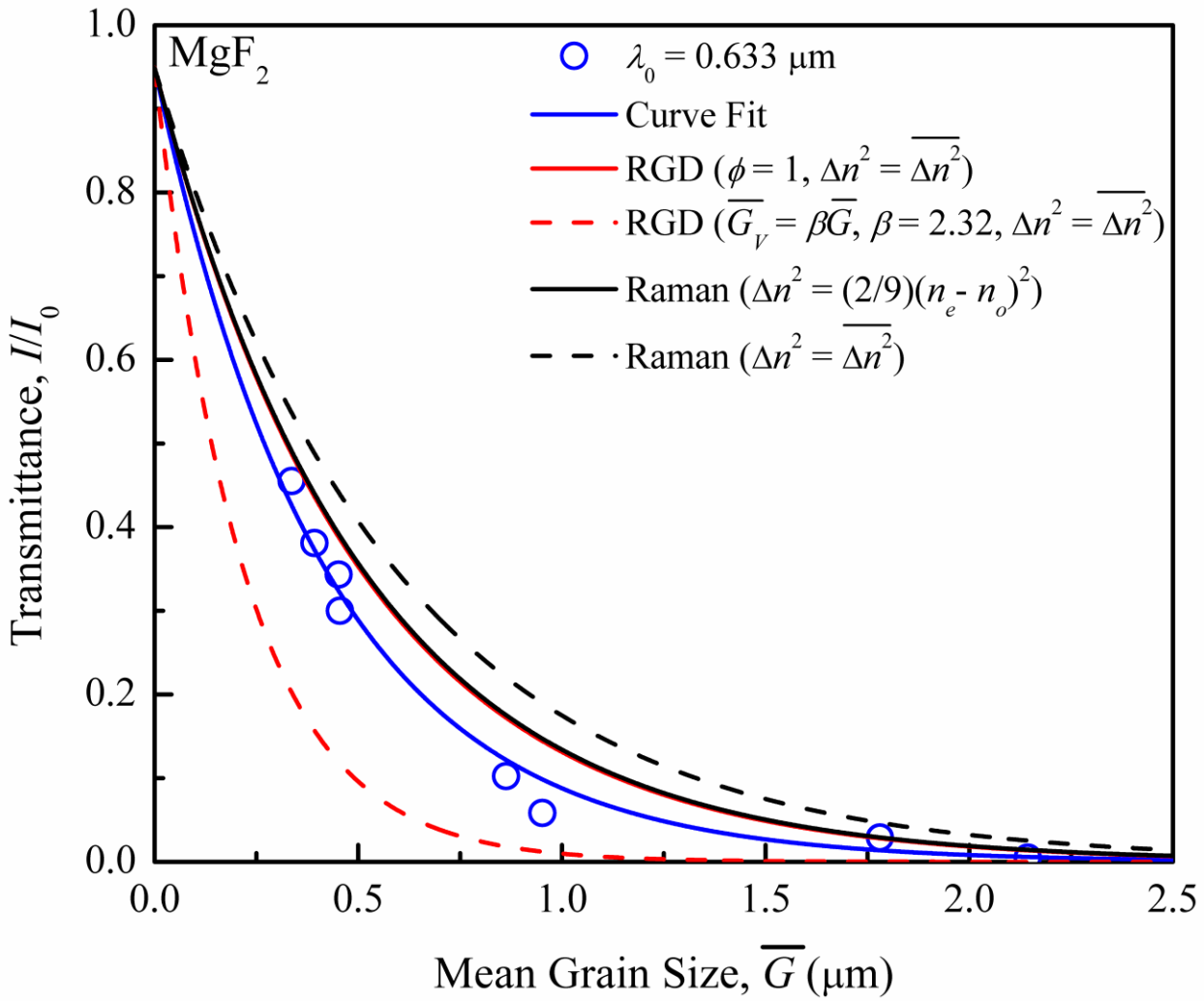

Figure 10. Transmittance of polycrystalline MgF_2 as a function of grain size compared with theoretical predictions.